Nano Scale Disruptive Silicon-Plasmonic Platform for Chip-to-Chip Interconnection

Demonstration of SPP amplifiers with electrical injection exhibiting 10dB/cm gain

Milestone no.:	M24
Due date:	06/30/2015
Actual Submission date:	07/31/2015
Authors:	IMEC, UGENT, UVEG
Work package(s):	WP4
Distribution level:	RE[1] (NAVOLCHI Consortium)
Nature:	document, available online in the restricted area of the NAVOLCHI webpage

List of Partners concerned

Partner number	Partner name	Partner short name	Country	Date enter project	Date exit project
1	Karlsruher Institut für Technologie	KIT	Germany	M1	M36
2	INTERUNIVERSITAIR MICRO-ELECTRONICA CENTRUM VZW	IMEC	Belgium	M1	M36
3	TECHNISCHE UNIVERSITEIT EINDHOVEN	TU/e	Netherlands	M1	M36
4	RESEARCH AND EDUCATION LABORATORY IN INFORMATION TECHNOLOGIES	AIT	Greece	M1	M36
5	UNIVERSITAT DE VALENCIA	UVEG	Spain	M1	M36
6	STMICROELECTRONICS SRL	ST	Italy	M1	M36
7	UNIVERSITEIT GENT	UGent	Belgium	M1	M36

[1] **PU** = Public
PP = Restricted to other programme participants (including the Commission Services)
RE = Restricted to a group specified by the consortium (including the Commission Services)
CO = Confidential, only for members of the consortium (including the Commission Services)

Deliverable Responsible

Organization: imec
Contact Person: Dries Van Thourhout
Address: St. Pietersnieuwstraat 41
9000 Gent
Belgium
Phone: +32 9 2643438
E-mail: dries.vanthourhout@ugent.be

Executive Summary

This extended milestone document summarizes the results obtained during the last reporting period towards achieving active integrated waveguide devices (amplifiers and lasers) based on colloidal quantum dots integrated with dielectric layers.

The objective of this subtask within NAVOLCHI, WP4 was to develop an integrated waveguide amplifier using colloidal quantum dots (CQD) as the active material. This required development of new types of CQDs exhibiting gain in the telecom wavelength range, new waveguide platforms allowing to couple light emitted by the CQDs efficiently to an optical cavity or amplifier and an electrically injection scheme. All of these subtasks were completed succesfully:

- Using a novel material, HgTe, we demonstrated for the first time CQDs exhibiting long-lived gain with ultralow threshold fluence in the wavelength range 1100nm-1600nm. A gain of 100cm-1 is extracted from the measurements (for a close-packed film) . These results are described in section 2.
- We developed new platforms, SiN and PMMA based, which allow efficient coupling of CQD-emission to integrated waveguides. We demonstrated gain and lasing in amplifiers and disk resonators fabricated in these systems. These results are described in section 3 and 4.
- We demonstrated light extraction from electrically injected stacks of SiN with embedded CQDs

Unfortunately, we did not yet manage to combine all these results in a single device thus far. However, we strongly believe the results achieved in NAVOLCHI form the basis for achieving this in the near future and research towards achieving this continues.

Change Records

Version	Date	Changes	Author
0.1 (draft)	2015-06-30	Start	Dries Van Thourhout Pieter Geiregat Suzanne Bisschop Weiqiang Xie Yunpeng Zhu Juan Pastor I. Suarez
1 (submission)	2015-02-9		Dries Van Thourhout

1 Introduction

This extended milestone document summarizes the results obtained during the last reporting period towards achieving active integrated waveguide devices (amplifiers and lasers) based on colloidal quantum dots integrated with dielectric layers.
First we describe the most recent progress in developing HgTe colloidal quantum dots (CQDs) as a novel gain material for applications in the NIR wavelength range (section 2).
Next we describe the integration of colloidal quantum dots in two types of dielectric waveguide systems (SiN, section 3 and polymer, section 4), and the characterisation of devices fabricated in these waveguide platforms.
Finally we describe results on light extraction from electrically injected stacks incorporating CQDs (section 5).

2 HgTe: a novel gain material in the telecom wavelength range.

2.1 Introduction

Tuneable, low cost and solution processable gain media could have a large impact on devices relying on optical gain, such as lasers or amplifiers. Taking the example of the telecom wavelengths around 1.3 and 1.55 μm, lasers are now mostly fabricated through expensive epitaxial growth of III-V semiconductors. In the case of the popular silicon photonics platform, whereby densely packed photonic integrated circuits are fabricated starting from silicon-on-insulator (SOI) for applications in classical data communication but also for signal processing and sensing, this implies that no native gain medium is even available. Solutions relying on bonding of III-V dies, direct epitaxial growth of III-V on silicon, erbium doping and strained Ge are heavily investigated but suffer from cost, upscaling and efficiency issues or limited gain bandwidth. Although stimulated emission involving the bandgap transition has been demonstrated for different colloidal quantum dots (QDs), their use as gain media has been limited. This is largely due to the QDs being effective two-level systems, where stimulated emission and absorption involve transitions between the same discrete band edge states. Since these are degenerate, the average number of excitons per QD, a number referred to further as <N>, must exceed unity to achieve population inversion. Next to this intrinsic drawback of two-level gain media, multi-X rapidly recombine through non-radiative Auger processes, limiting the gain lifetime to a few tens of picoseconds. Although the resulting high thresholds can be reached by optical pumping using pulsed lasers, it makes electrical pumping of QD-based gain media infeasible. Two strategies have been proposed to circumvent the limitations imposed by multi-X gain. It proved possible to slow down Auger recombination through interfacial alloying in core/shell QDs and/or using large volume QDs. Alternatively, single-X gain has been demonstrated using so-called type II core/shell QDs, where the spatial separation of electron and hole leads to repulsive X-X interactions, lifting the effective level degeneracy. Unfortunately, both strategies are restricted to a few materials – typically involving Cd-based QDs emitting in the visible – and gain still relies on a two level scheme. Here, we report on optical gain in dispersions of HgTe QDs with average exciton numbers per nanocrystal $\langle N \rangle$ as low as 0.005. Intrinsic gain coefficients of about 500 cm^{-1} are demonstrated and the extrapolated gain lifetime corresponds to the single exciton lifetime. We attribute this almost thresholdless gain to stimulated emission between the lowest conduction band level and shallow, empty surface states near the first valence band level, thus creating a nearly thresholdless, effective 3-level system. Since the gain characteristics meet the requirements for DC electrical pumping, this result shows that the use of effective 3-level systems is the way forward for developing performing QD-based gain media.

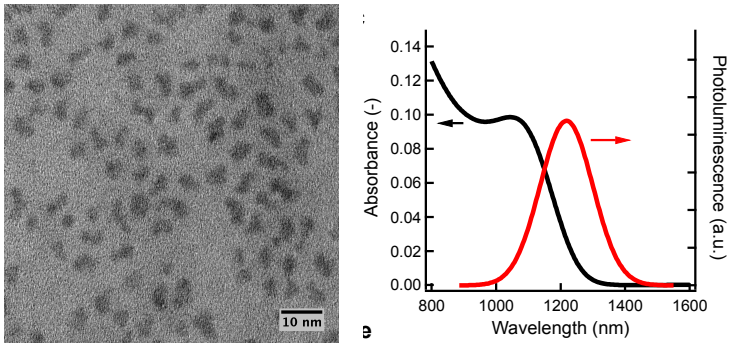

Figure 1 (left) HgTe nanocrystals on a TEM grid for structural analysis and (right) absorbance and photoluminescence (with 700 nm CW photoexcitation) spectrum of 3 nm QDs.

2.2 Transient Absorption Spectroscopy

HgTe is a II-VI compound that stands out since it is a semi-metal with a direct negative bulk bandgap. As a result, the HgTe bandgap can be tuned from the long-wave infrared down to the near-infrared by means of size quantization (see Figure 1), where bandgaps up to 1 eV can be reached with 3 to 4 nm nanocrystals. This allows us to cover the near-infrared window of 1.3 to 1.55 micrometre with small changes in the reaction chemistry. We analyzed optical gain in dispersed colloidal HgTe QDs using broadband transient absorption (TA) spectroscopy. This involved the excitation of a QD ensemble using a 180 fs laser pulse at 700 nm, followed by probing the change in absorbance $\Delta A = A - A_0$, where A is the absorbance after photo-excitation and A_0 the absorbance in absence of the pump pulse, as a function of wavelength and pump-probe temporal delay. TA measurements are represented by the normalized absorption change ($\Delta A/A_0$) or the non-linear absorbance $A = \Delta A + A_0$, the more useful quantity when evaluating amplification. Bleaching (*i.e.*, reduction) of the absorption, either through state-filling or spectral shifts corresponds to $\Delta A < 0$, while photo-induced absorption, either through intraband absorption or spectral shifts corresponds to $\Delta A > 0$. Note that the occurrence of optical gain at a given wavelength is evidenced by $\Delta A < -A_0$, or, equivalently, a negative non-linear absorbance $A < 0$. In that case, the sample emits more photons than it absorbs, *i.e.*, stimulated emission dominates over absorption.

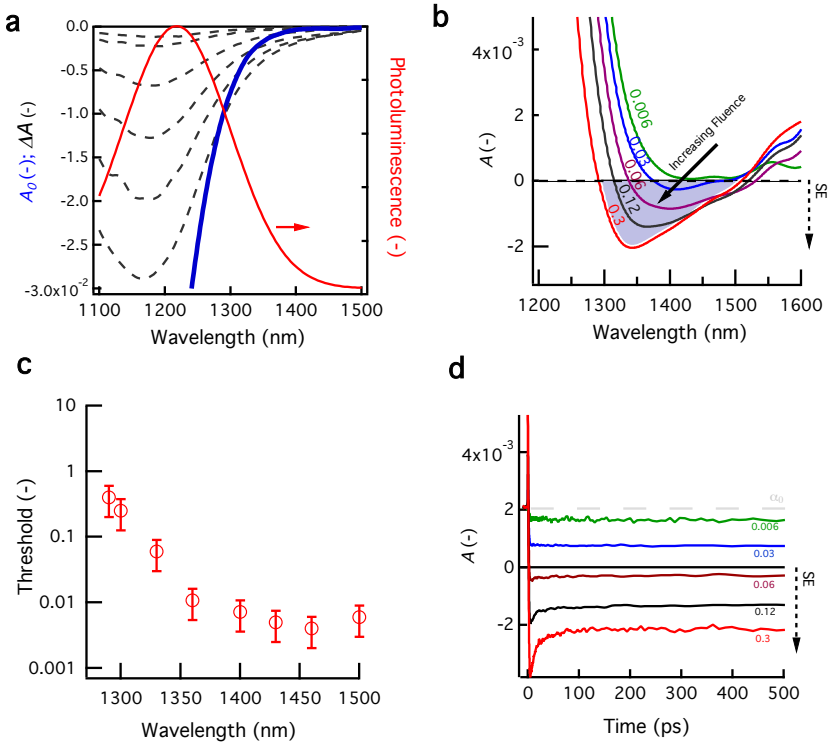

Figure 2 Analysis of fluence dependence (a) Fluence dependent difference spectra ΔA (grey dashed line), taken 2.5 ns after photo-excitation at 700 nm, plotted together with the linear absorption A_0 (solid blue line) and emission (solid red line). (b) Non-linear absorption spectra *A*, again taken 2.5 ns after photo-excitation. Stimulated emission (SE) corresponds to A < 0. The maximum gain bandwidth extends from 1310 to 1500 nm at sub-X fluence (<N> = 0.3). (c) The wavelength dependence of the gain threshold as obtained from figure 3b (see text). (d) Kinetics of *A* at 1340 nm (gain maximum) for increasing fluence.

Figure 2 compares the corresponding bleach measured at a 2.5 ns delay for different pump fluences – increasing <N> from 0.006 to 0.3 – with the linear absorption and photoluminescence spectrum. It follows that at the long wavelength side a situation where $\Delta A > A_0$ is reached, *i.e.*, the sample amplifies the probe light, even for very low pump fluences. To make this observation more clear, Figure 2b plots the spectrum of the nonlinear absorbance A again measured for a 2.5 ns delay, for different pump fluences. Note that this delay strongly exceeds the lifetime of multi-X, such that QDs contain a single exciton at the most. At low fluence, $(\langle N \rangle < 0.006) < 0.006$, absorption dominates and A > 0 at all wavelengths. However, when increasing the fluence, A clearly becomes negative in a small spectral region. Increasing the fluence further, yet remaining well below $\langle N \rangle = 1$, the threshold in classical systems, broadens this gain region from 1290 nm to 1510 nm, covering 3 technologically relevant transparency windows of commercial glass fibre (O,E and S-band, 1260 to 1530 nm, see also Figure 3). From Figure 2b, we can derive the threshold for stimulated emission as a function of wavelength. This is displayed in Figure 2c, which clearly shows that the threshold for optical gain is far below the single exciton occupation ($\langle N \rangle = 1$), dropping to 0.005 at 1500 nm. Note that this is, to the best of our knowledge, the lowest gain threshold ever reported for colloidal QDs, both in the visible and near-infrared part of the spectrum.

To confirm the single exciton character of the observed optical gain, we analyze the decay of the bleach signal, *i.e.*, the gain lifetime. If the gain effectively occurs in the single exciton regime, the decay should be on the order of the luminescent lifetime, *i.e.* 30-40 ns. Representative kinetic traces (at 1340 nm) are shown in Figure 2d. As we know from the previous analysis, increasing the fluence renders *A* negative at populations far below $\langle N \rangle = 1$. More importantly however, the stimulated emission appears to be constant and persists longer than the measurable time window of the TA setup (2.5 ns). A fit to the apparently constant (in reality very slow) decay yields a lifetime of 34 ns, close to the measured 40 ns lifetime of single X. These findings confirm that the stimulated emission we observe is indeed due to singly excited QDs and no multi-excitons are involved.

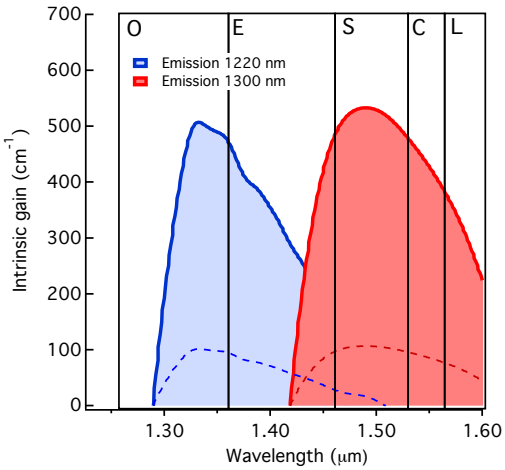

Figure 3 HgTe intrinsic material gain for two different samples emitting at 1220 nm (blue) and 1300 nm (red). The color-matching dashed lines indicate the volume-fraction corrected material gain. Note that the material gain provided by only 2 different sizes of HgTe covers the entire OESCL band with typical values over 100 cm^{-1}.

2.3 Intrinsic material gain

In the case of HgTe QDs, a model was built that the observed nearly thresholdless gain is related to a transition of a conduction-band electron to a shallow, empty gap state. This leads to a concise 3-level picture in line with the experimental data. The gain thresholds reported here for HgTe QDs are the lowest ever for optical amplification using colloidal materials – outperforming by 2 orders of magnitude the best Cd-based structures available in the visible range of the spectrum – and the gain lifetime exceeds that of multi-exciton gain by 3 orders of magnitude. Still, the question remains whether an effective 3-level system like HgTe QDs, where gain involves a transition to a gap state, can provide the modal threshold gain needed to achieve lasing when embedding the QDs in a feedback structure. To answer this question, Figure 3 shows the intrinsic gain coefficient g_i of 2 different batches of HgTe QDs, emitting at 1220 nm and 1300 nm. Actual gain coefficients are obtained by multiplying g_i with the QD volume fraction *f*, which amounts to 0.2 – 0.3 in a close packed film of dodecanethiol capped HgTe QDs (Figure 3 dashed lines). One sees that gain coefficients of 100 cm^{-1} are achieved across the entire telecommunication window (indicated with the standard pass bands O/E/S/C/L). These values lie between the gain obtained in erbium-doped fiber amplifiers (EDFA) used in C-band telecommunication (10^{-2}-10^{-3} cm^{-1}) and that of common epitaxially grown semiconductors (10^{3} cm^{-1}) used in integrated photonics, making HgTe a suitable material for both fiber based and integrated amplifiers. Moreover, the combination of gain threshold, gain lifetime and gain coefficients of 100 cm^{-1} make HgTe QDs a very promising gain material for integrated photonics, where in particular electrically pumped devices become feasible. Indeed, as mentioned by Wood et al. gain lifetimes of ca. 100 ns are required at sub-1 exciton population to achieve DC electrical pumping specifications that are largely met by the colloidal HgTe QDs used in this work.

2.4 Towards integration: thin film formation and properties

The ultrafast properties of HgTe described above are obtained on solutions of HgTe QDs colloidally dispersed in apolar solvents. To translate these exciting properties (low threshold, long gain lifetime and large gain magnitude) to an actual integrated amplifier or laser, we should process the QDs into thin films. Employing the same transient absorption routine as outlined above, we observe a decreased performance of HgTe QDs in the thin spincoated films used in these experiments (see Figure 4). Although gain is still observed at exciton densities below unity, the thresholds are substantially higher (up to 1 order of magnitude) and the cross sections are smaller. The gain lifetime is however still of the same order as in the solution case. We attribute this decrease in gain cross section to increased photocharging (*i.e.* unbalanced charges agglomerate in the film which unable to vanish) which induces a photo-induced absorption (mainly due to a type of intraband absorption) overwhelming the gain signal. This could be an inherent problem as we attributed the 3-level structure that gives thresholdless gain to surface traps, a known source of such photo-charging. As such, these traps are therefore a gift and a curse at the same time.

Although these results are somehow shadowed by their solution counterparts, the measurements still show that we obtained optically pumped low threshold amplification of near – infrared light (in this case the probe), a absolute premise for an amplifier or laser.

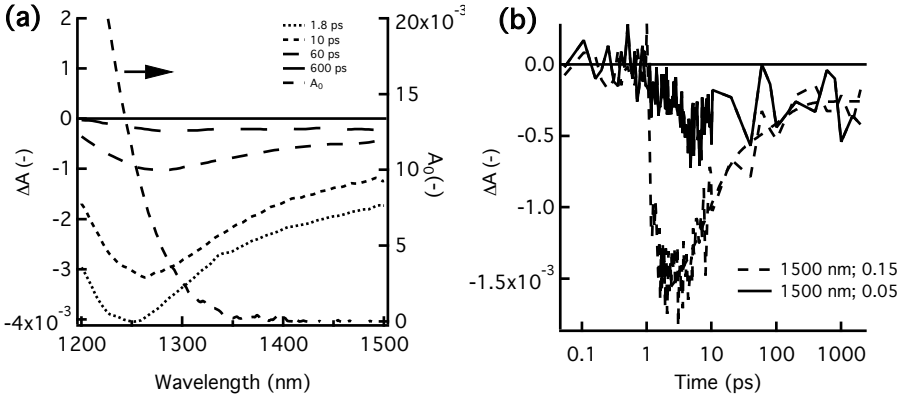

Figure 4 Overview of HgTe thin film measurements: (a) Bleach spectra for different probe delays at <N> = 0.5 and (b) Bleach kinetics at 1500 nm for 2 different fluences (0.05 and 0.15). The dashed black line is a biexponential fit yielding a 8 and 100 ps lifetime respectively.

As we concluded, the photocharging and the subsequent decreased performance of HgTe QDs in thin film phase is attributed to charge accumulation due to surface traps and clustering of the QDs. The HgTe QDs are capped with thiol-based ligands (dodecane-thiol as standard). These ligands are known to show clustering and their metal-complexes (*e.g.* mercury-thiolates) are known to show long range ordering in solid phase. The latter can be present in the synthesis solution through reaction of thiols with the mercury chloride. In the first synthesis route, thiols are added from the beginning, together with the mercury chloride. In the second route, thiols are only added during workup, but still unreacted mercury chloride can be present. It was suggested by others that these mercury-thiolates form a gel-like network clustering together a few QDs in a 10-20 nm clusters. We observed similar cluster sizes using DLS (Dynamic Light Scattering). They attribute photo-charging of the QDs to the presence of these clusters (e.g. trapping of carriers in the interconnected and rather ionic network). As such, breaking them apart in future work could improve the performance of HgTe as we attributed the gain reduction at high fluence to this photocharging.

2.5 Integration of HgTe thin films into DBR cavities

Although the performance of HgTe dots is decreased in thin films, we still attempted to construct an actual optical feedback structure around the films to create an optically pumped 'laser'. The feedback is provided by 2 mirrors, here made as distributed bragg reflectors (DBR) of alternating low index silicon nitride (SiNx, n = 2.1) and high index amorphous silicon (a:Si, n = 3.3). Due to the large index contrast we only need to grow about 5 pairs of SiNx/a:Si to achieve broadband >98.5% reflection of a single mirror (see Figure 5) in the near-infrared.

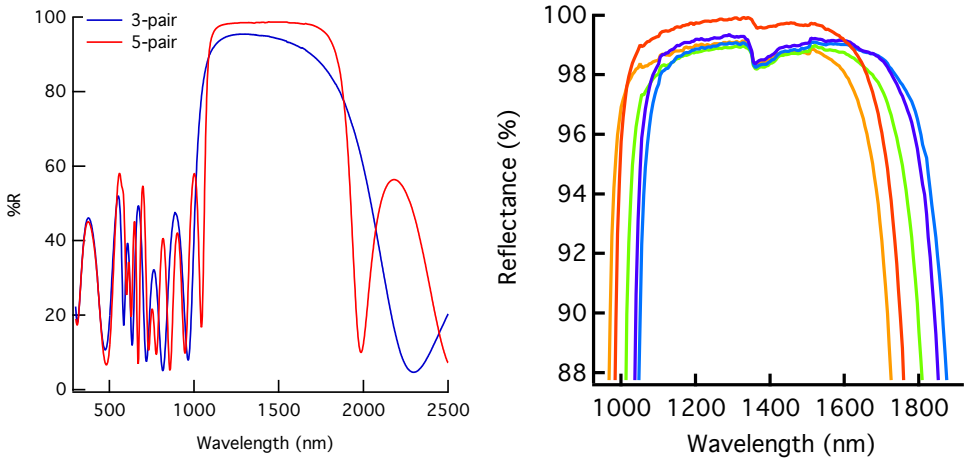

Figure 5 (left) Reflection under 8° incidence of 3 and 5-pair a:Si/SiNx DBR mirror and (right) reproducibility of mirror fabrication over 5 runs showing detail of high and broadband reflection in the telecom range where HgTe QDs exhibit optical gain.

HgTe QDs are dropcasted on one mirror and dried under nitrogen. Next, the mirror is glued to a secondary mirror using a two-component epoxy mixed with silica spacer balls of varying thickness (from 5 to 100 micron). Samples are excited under normal incidence using a CW laser at 800 nm and the photoluminescence is collected under similar normal incidence conditions. Figure 6 shows a preliminary result where spontaneous emission in free space (black solid line) is clearly altered by presence of the cavity (blue line). Future work will focus on improving the cavity thickness and quality of dropcast films in combination with pulsed laser excitation to show a near-infrared solution processable laser based on HgTe QDs.

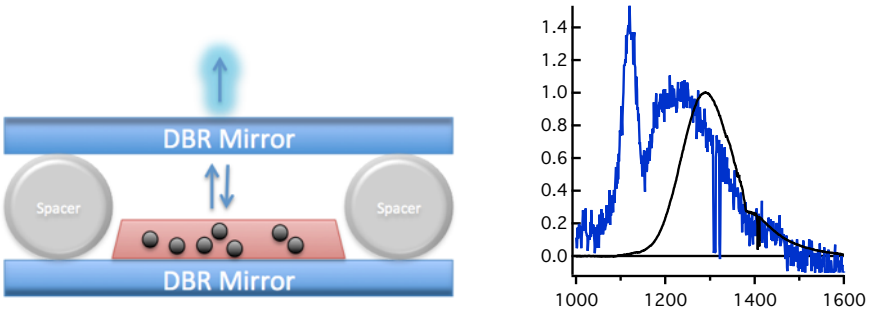

Figure 6 (left) Schematic of fabricated DBR feedback cavity and (right) first results showing the emission of a cavity (blue) compared to the free space emission (black) coupling of QD spontaneous emission to one of the cavity modes (for a cavity spacer 5 micron).

3 Hybrid SiN-QD waveguides and cavities

3.1 Introduction

Given its moderate optical index (~2.0), broad operating wavelength range and low-loss, silicon nitride (SiN) forms a promising platform for various applications including integrated photonic circuits [1], nonlinear optics [2], and on-chip biosensing [3]. On the other hand, because of its dielectric nature, SiN devices have thus far been limited to passive functionalities and an optically active SiN photonics platform is highly desired. One of the possible choices is to combine gain material with SiN building blocks such as waveguides and resonators [4][5] for making active devices – e.g. a laser or a single photon emitter. As a novel class of materials, colloidal quantum dots (QDs), with their efficient and broadly tunable luminescence, are an ideal candidate for integration with SiN

photonics. An efficient integration process should preserve the optical properties of the QDs and allow realization of low-loss SiN circuits. More importantly, to enable effective coupling between the QD emission and waveguide or cavity modes, these modes should maximumly overlap with the QD emitters. In practice, it is also important that these active SiN-QD devices are combined with low loss passive access waveguides that allow combining multiple devices or coupling the generated light of chip. In this work, we developed a fully inorganic, low-loss SiN-QD hybrid photonics platform by using low-temperature (270°C) plasma enhanced chemical vapor deposition (PECVD) and optimized reactive ion etching (RIE) processes. Based on this platform, we designed and fabricated free-standing SiN microdisks with colloidal QDs embedded inside, and coupled them vertically with on-chip SiN bus waveguides. Efficient coupling of QD photoluminescence (PL) to disk modes is experimentally demonstrated. Under higher pumping power we now also for the first time noted spectral narrowing and possibly even lasing. Next to the disk resonators we also demonstrated QD-embedded straight waveguides and demonstrated ASE (amplified spontaneous emission) from these waveguides. These high-performance active SiN-QD devices open up new opportunities for both QD-based quantum optics and SiN-based photonic applications.

3.2 QDot characterization

The QD used in this work are different types of the recently developed (UGENT) "flash" CdSe/CdS core-shell colloidal quantum dots (QDs). These types of dots have large CdS shells, which create an improved surface passivation, while on the other hands they also have alloyed interfacial layers, which provide more smooth wave functions of electrons and holes. The smooth wave function created by the alloyed interfacial layer weakens the Auger recombination. We performed pumping experiments for drop casted compact layer on glass substrates and under pulsed, high power laser pumping (1kHz repetition rate @ 20mW) the QD compact layer shows amplified spontaneous emission (ASE). Figure 7 shows a typical the emission spectrum under the pulsed laser pumping, showing spectral narrowing and ASE peaks both at 600nm (S-S transition) and at 530nm (P-P transition).

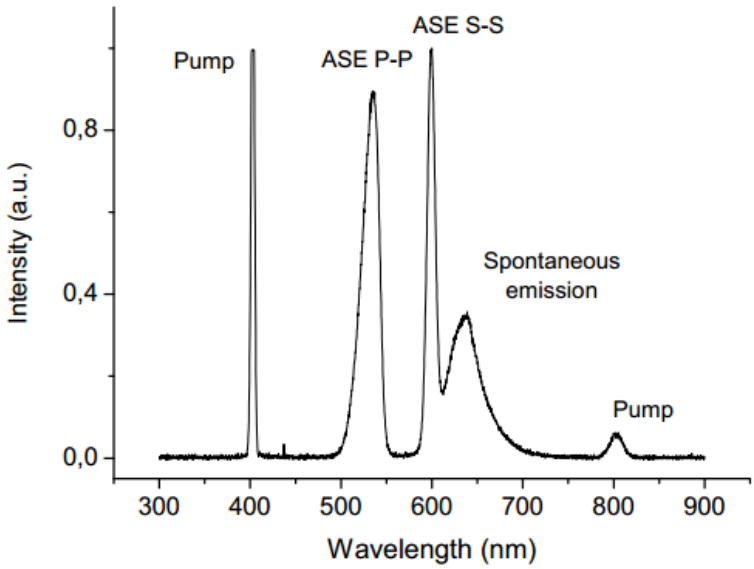

Figure 7 Emission spectrum of drop cast compact layer of "flash" QDs under pulse laser pumping

3.3 Design and fabrication disk resonators

The design of the SiN-QD disk with vertically coupled waveguide is shown in Figure 8. The bus waveguide is defined on a silicon wafer with a 3µm SiO_2 layer and is also sideways embedded in SiO_2. An amorphous silicon (aSi) pillar supports the SiN disk with the embedded QD layer. The height of the aSi pillar determines the vertical coupling gap between the disk and the waveguide. The undercut distance *d* is chosen sufficiently large to prevent leakage of the fundamental transverse electric (TE) modes to the aSi pillar. To tune the coupling strength, the horizontal offset between the center of the bus waveguide and the edge of the disk is adjusted from -400 nm to +400 nm, with positive offsets denoting a bus waveguide closer towards the centre of the disk.

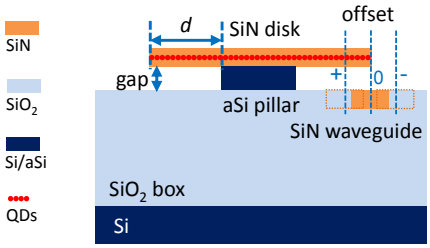

Figure 8 Cross-sectional schematics of device design.

From finite-difference time-domain simulations, we choose a height of ~135 nm for the bus waveguide, guaranteeing single mode operation at a wavelength of 625 nm, the peak PL wavelength of the QDs employed. The disk height was set at ~180 nm to ensure low-loss for the TE-like disk modes. The width of the bus waveguide and the diameter of the SiN disk were varied to study their influence on the disk-waveguide coupling. The vertical coupling gap was fixed at ~200 nm. Note that there are two main advantages to our vertical coupling configuration. First, it allows for an on-chip waveguide-coupled free-standing disk and therefore to achieve high quality (Q) whispering gallery modes (WGM) with low radiation loss, even for relatively small diameters. Second, because of the separation of the fabrication steps for waveguide and disk, we can integrate the QDs exclusively in the disk and not in the access waveguides. This allows to study the coupling of the QD emission to disk modes without background interference, which would not be possible if also the waveguides contain QDs as would be unavoidable in a lateral coupling scheme.

The fabrication starts with the deposition of a ~135 nm PECVD SiN layer onto a wafer with a 3 µm thermal SiO_2 box layer. Next the bus waveguide is patterned using contact lithography and RIE etching to form a strip waveguide. Both the contact lithography and the RIE process were optimized to be able to define a low-loss waveguide supporting only a single TE-like mode at the operating wavelength. This ensures only the TE-like disk modes are coupled out efficiently. After waveguide fabrication, a 800 nm PECVD SiO_2 cladding is deposited and a chemical mechanical polishing step is applied down the top of waveguide layer to planarize the surface, as shown in Figure 8. Next, the vertical coupling gap is defined by depositing a 200 nm thick PECVD aSi layer. The SiN-QD composite layer is prepared by first depositing a ~90 nm SiN layer, then spin-coating a nearly monolayer of QDs, and then depositing another ~80 nm SiN layer on top of the QDs. These latter ones consist in 10 nm CdSe/CdS core/shell QDs prepared according to the "flash" synthesis procedure [6]. The disk is defined using the same process as used for the waveguides. Finally an alkaline based wet etch is utilized to undercut the aSi and to realize the free-standing SiN-QD disk schematically depicted in Figure 8. The microscope and SEM pictures of Figure 9(a-c) show the designed structure is accurately realized.

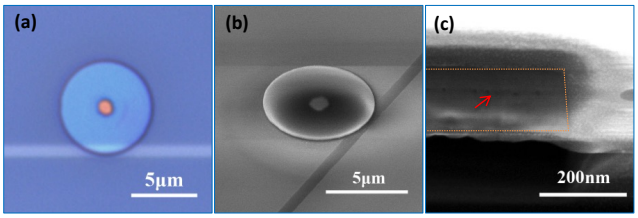

Figure 9 (a) Optical and (b) scanning electron microscope images of one fabricated device with a 7µm diameter disk. (c) Cross section of the etched profile of disk with the red arrow indicating the embedded QDs.

3.4 Characterization Results Disk Resonators (low excitation)

We characterized the PL spectrum of the fabricated devices, first at low pump powers. A 400 nm pulsed femtosecond laser was used for pumping the disk from the top and the PL-signal was collected from the cleaved facet of the bus waveguide using microlensed fibers. In Figure 10, we show the normalized PL spectra of disks with various radii coupled to a ~500 nm wide bus waveguide with an offset of about -160 nm. The envelope of these PL spectra arises both from the wavelength-dependent emission of the QDs (inset of (a)) and from the wavelength-dependent disk-waveguide coupling. The spectra clearly show the TE WGM modes and the background PL signal is very strongly suppressed. This can be attributed to the enhanced interaction between the QDs and the disk modes and the efficient coupling of the disk modes to the access waveguide. Since the location of the QDs is aligned with the maximum of the light field in the disk we can boost the interaction between them and improve the coupling efficiency of the QD emission into the disk modes. In Fig. 3(a-d), we also denote the Q-factors of the resonances around 625 nm obtained by fitting a Lorentzian. We obtain a Q of 1160 with a free spectral range (FSR) of ~8.8 nm for the 3.5 µm radius disk and a Q of 5740 with a ~3.0 nm FSR for the 10.0µm radius disk. Note that characterization of the modes with Q above ~4000 is already limited by the 0.05 nm resolution of the spectrometer

we used and an even higher actual Q is therefore expected for the 10.0 μm radius disk. In Figure 10(c) and even more so in Figure 10(d), the second order TE mode family also starts to appear. By increasing the width of the bus waveguide, we can reduce the undesired coupling of the second order TE modes, as shown in the inset of Figure 10(d). The coupling strength for a certain mode family can also be tuned by changing the offset (not shown here), illustrating further the advantages of the vertical coupling scheme.

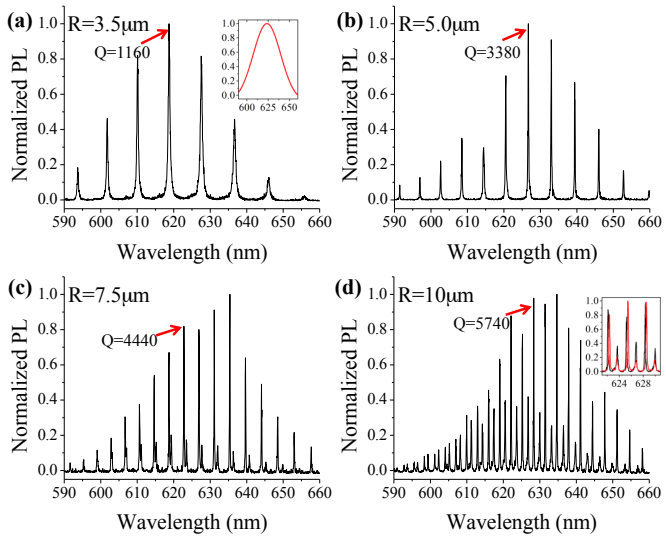

Figure 10 (a-d) Normalized PL spectra of the devices with different radius disks coupled to ~500 nm wide waveguides under an offset of around -160 nm. Red arrows designate the first order TE modes around 625 nm together with the fitted Q. The inset in (a) shows the PL from slab waveguide for reference. The inset in (d) presents two PL spectra coupled out from different bus waveguides with widths of ~500 nm and ~670 nm for the black and red curves, respectively.

3.5 Characterization Results Disk Resonators (high excitation)

To study possible lasing of these devics, we also developed processes for integration of a thicker QDs layer. The design and fabrication are similar to that described above except for the pillar part. Here the top disk is supported on the planarized SiO_2 surface. The presently developed process allows for integrating thick QDs (30-100nm) within SiN disk and in Figure 11 we show the fabricated device with ~55nm thick CdSe/CdS core/shell QDs embedded in SiN disk. Again we used a focused beam (spot size ~100μm diameter) to pump the disk from the top and collected PL from the cleaved facet of the access waveguide using microlensed fibers. In Figure 12 we show the normalized PL spectra of disk pumped with two different laser beams denoted "MAITAI" and "TOPAS". Here, "MAITAI" is a 80 MHz femtosecond Ti:Sapphire laser at 400nm, and "TOPAS" is a 1 kHz amplified system with higher pulse energy at 450nm. From Figure 12(a), it is clearly seen that spontaneous emission of QDs is coupled to the whispering gallery modes (WGM) of the disk and the background PL signal is quite small, since the location of QDs are perfectly aligned with the maximum of the light field in the disk, resulting in an efficient coupling of the QD emission into the disk modes. Note that the envelope of the PL spectrum in Figure 12(a) arises from the wavelength-dependent spontaneous emission of the QDs. When pumping with TOPAS, as shown in Figure 12(b) the PL spectrum shows significantly different features compared to the pumping with MAITAI. The narrowed-down spectrum envelope (~10nm width) is clearly observed and only a few of the WGM modes are remained. This narrowed-down spectrum might be from the ASE of QDs. However, the pump-power dependent and time-resolved PL measurements are further needed to investigate the narrowing effect of the spectrum and the characteristics of these disk modes.

In Figure 13(a), we show the PL spectra of the disk of 15 μm diameter pumped with different power of TOPAS. Again we observe the narrowing feature of the spectra similar to the 20 μm diameter disk. On the other hand, the intensity of the spectra shows evident sensitivity to the pump power and it increases rapidly from 0.02 to 0.03mW pump power while decreases when further increasing the pump power to 0.15mW. In Figure 13(b), we plot the integrated PL intensity as a function of pump power and it is even clear that the overall output PL power gains sharply and then decays gradually as strengthening the pump power. The preliminary results show possible lasing effect in QD-SiN disk and detailed measurement at low pump power (below 0.03mW) is needed to confirm whether lasing occurs at a certain threshold pump power. At higher pump power region a saturation output power is expected while a reduction of PL is actually observed. This could be attributed to heating effect of the disk when increasing the pump power; however it still needs to be investigated.

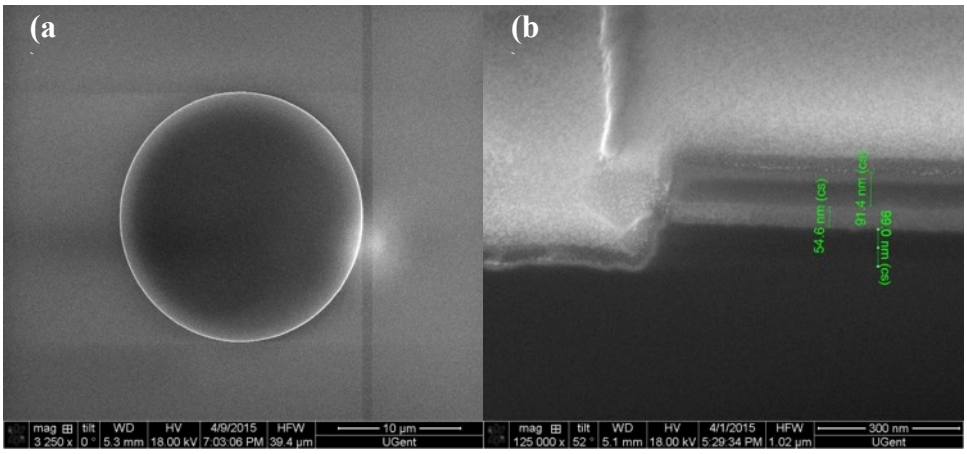

Figure 11 (a) SEM image of the top view of fabricated disk with a diameter of 20 µm and (b) cross section of the etched profile of disk with ~55nm thick QDs embedded in SiN disk.

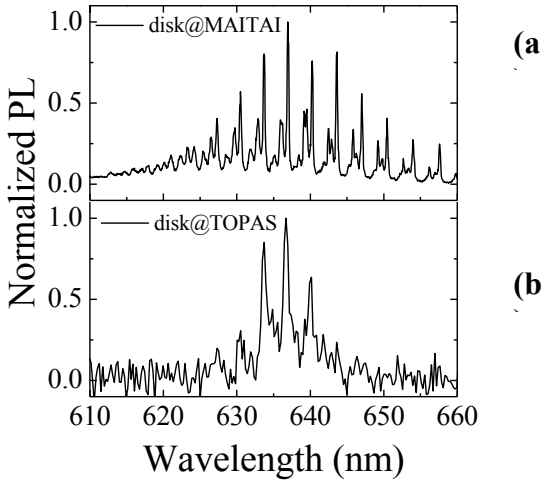

Figure 12. (a) and (b) PL measurement results of SiN disk with a diameter of 20 µm pumped with different laser beams.

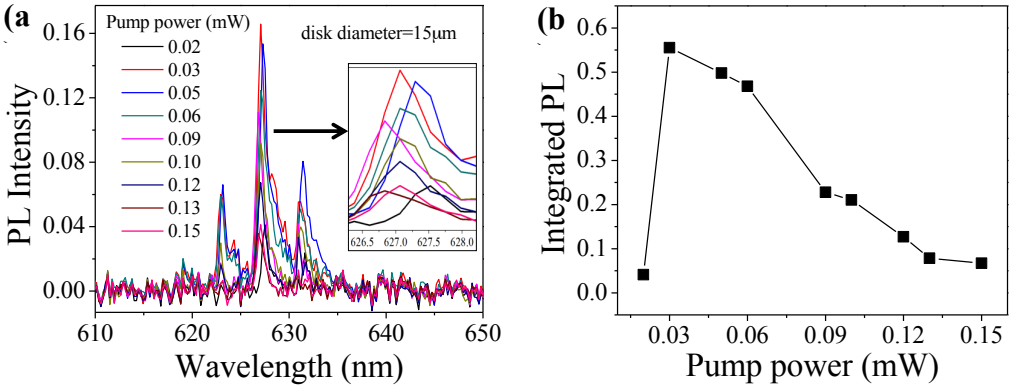

Figure 13 (a) PL spectra under different pump power of TOPAS. (b) Integrated PL intensity as a function of pump power.

3.6 Characterization Results In-line amplifiers (high excitation)

Next to the resonator devices we also investigated straight waveguides with embedded QDs. Again we first used PECVD to deposit 100nm high temperature low frequency SiN layer on top of SiO2. The measurement shows this type of SiN has quite low optical loss which is the reason we choose it as the under layer. Then we spin coat one layer of "flash" QDs on top of the first layer. The layer thickness can be controlled by the concentration of the QDs solution and the spincoating speed. Here we used a 50nm uniform compact QDs layer. Then we deposited another 100nm high temperature mixed frequency SiN on top of the QDs layer. We choose this type of SiN because the stress of the layer is more or less compatible with the QDs layer underneath and hence peeling of the layer is avoided in these larger structures. Other types of SiN have different stress compared with QDs layer, which will cause the up layer crack after deposition. After one step of etching through the QDs layer, we can have the waveguide with embedded QDs in between.

We performed an measurement evaluatiog the excitation power dependence with this sandwich waveguide sample. A cylindrical lens is used to form a narrow line beam to pump along the waveguide, as shown in Figure 14. The emission is collected by a lensed fiber, the collected light has been measured by power meter and spectrum analyzer separately to obtain the power and spectrum information. Figure 15a shows the spectrum information of the collected light. The emission is around 520nm, which is consistent with the ASE P-P from the dropcast sample. Figure 15b shows the result of excitation power dependence of this waveguide with embedded QDs in between. There is a clear non-linear power dependence of the ASE, but also saturation at higher pump powers. Quantitative analysis of these results to extract a modal gain is currently under way.

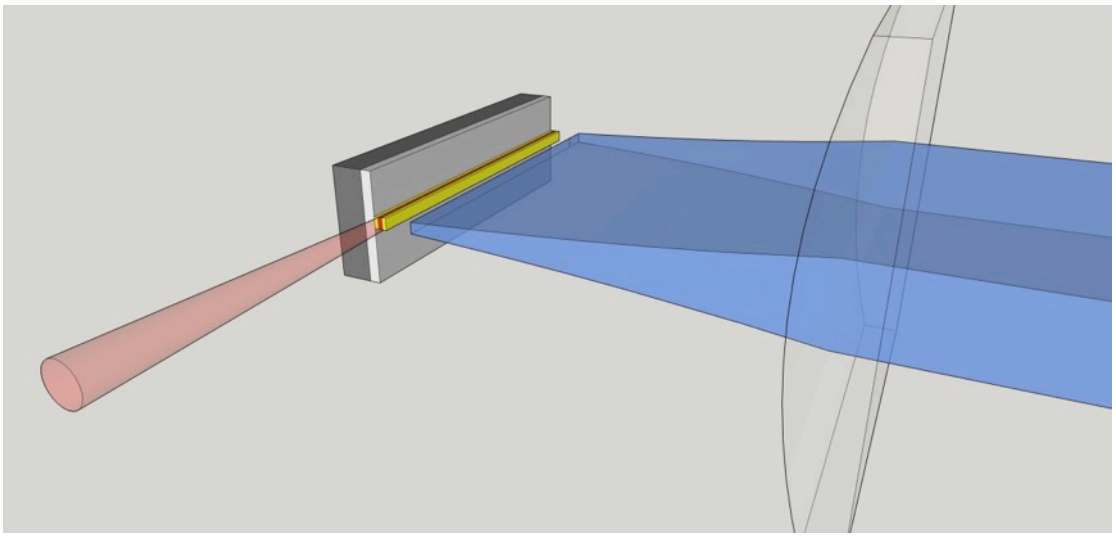

Figure 14 cylindrical pumping along the waveguide

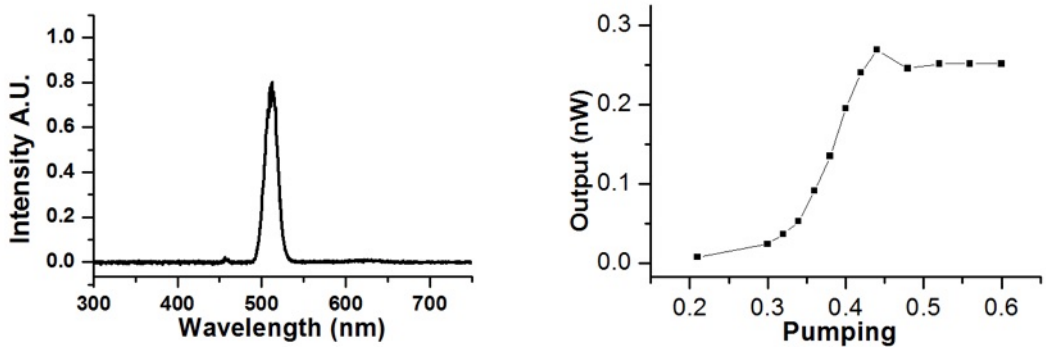

Figure 15 a) Spectrum of emission from waveguide facet. The small peak around 450nm coms from the pumping laser. b) Excitation power dependence measure

3.7 SiN-platform : Conclusion

The developed QD-SiN hybrid-platform developed is one of the first platforms providing active functionality (light emission) for a traditional purely passive, dielectric waveguide platform. Results are very encouraging but futher analysis is underway to proof actual laser operation (for disk resonator devices) and to extract the modal gain (waveguide devices).

4 Polymer QDOT devices

The new and promising QD-material (HgTe) developed by UGENT, whose synthesis and gain characterization in solution was discussed above, was also studied embedded into PMMA to form optical waveguides on a SiO_2/Si substrate, as depicted in Figure 16. In Structure I (Figure 16a) the QDs are dispersed homogenously in the PMMA matrix and in Structure II (Figure 16: b) a dense close-packed HgTe layer is deposited in between two PMMA layers. These waveguides were characterized by end-fire coupling and by the variable stripe length method in order to examine their waveguide photoluminescence, gain and losses (as similarly reported for other QD-materials in deliverable 4.1) under continuous wave (CW) and pulsed laser pumping conditions.

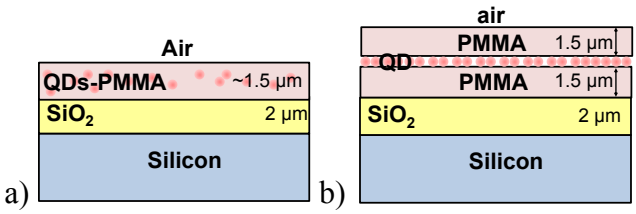

Figure 16: Waveguide structures studied: a) HgTe QDs dispersed homogeneously in a PMMA film and b) a dense close-packed HgTe QD layer sandwiched between two PMMA films. In both cases the polymers are deposited onto a SiO_2/Si substrate.

Qualitatively, waveguided photoluminescence intensity is stronger when using the HgTe-PMMA structure as compared to PbS-PMMA (previous QD-materials studied in the project). However, the initial gain (before saturation) deduced from experiments (Figure 17a) was smaller (250 cm^{-1} as compared to 350 cm^{-1} in PbS/CdS nanostructures). Concerning the losses (Figure 17b), both QD-materials gave similar values, due to the fact that they exhibit similar large stokes-shift and hence losses are presumably dominated by roughness scattering and not by reabsorption. Moreover, to obtain such values of gain it is necessary to use a high concentration of QDs in the polymer, which in turns restricts the propagation of the pump beam through the waveguide. This was the reason to propose the second structure in Fig. 16b, which allows the propagation of the pump laser (400 / 533 nm, particularly) through the PMMA cladding layers, where absorption from pump beam is absent. Intense waveguided PL is measured with structure in Fig. 16b, but a faster saturation is observed as compared to that of Fig. 16a. HgTe QDs seem to be a promising material for active purposes since it exhibits a large Stokes shift and dielectric waveguides exhibit a high amount of waveguided photoluminescence. Although dropped-casted QD layers seem to be unstable with temperature and illumination time, the photostability is rather high once QDs are incorporated into PMMA. In spite of these positive features, we do not observe any amplification effect in the dielectric waveguides prepared and studied, that is, still presenting gain saturation effects as measured with other previous QD materials.

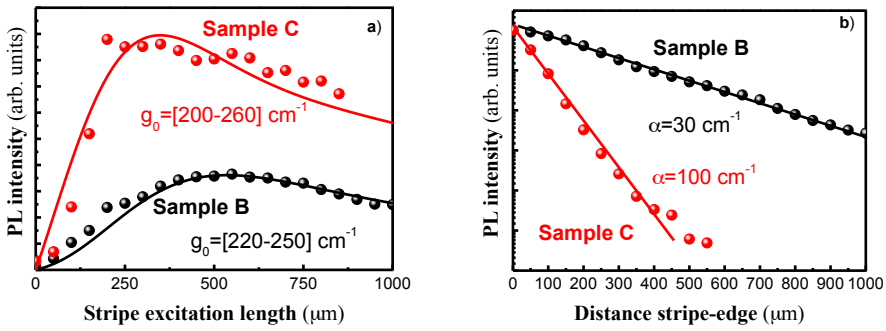

Figure 17: Peak photoluminescence (around 1000 nm) intensity as a function of the stripe excitation length (a, gain) and as a function of the distance between the stripe and the edge of the sample (b, losses). Samples A and B corresponds to QD filling factors of 0.008 and 0.08, respectively.

It is worth noting that dielectric waveguides are good candidates to combine with solution processed active materials, not only QDs. Very recently we probed amplification of the spontaneous emission at around 780 nm [7], by combining Lead Halide Perovskites (HPVK) with a PMMA cladding, as shown in Figure 18. These materials are very promising for active photonics in silicon platforms, eventually combined with QDs to obtain different emission wavelengths, as recently probed by Sargent and co-workers [8].

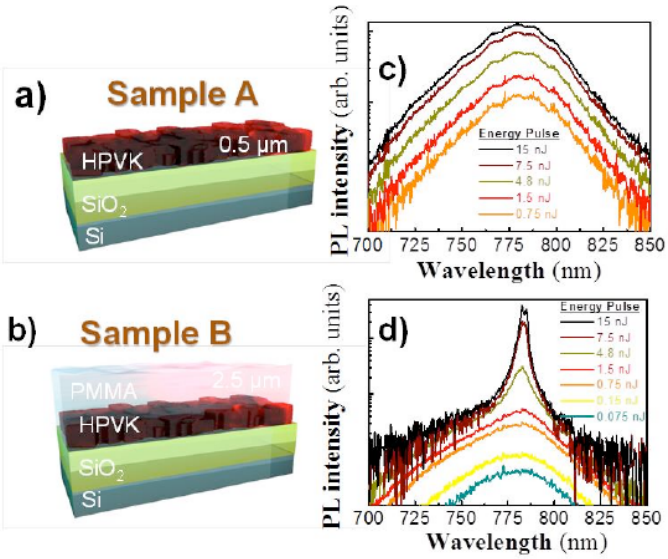

Figure 18: (a) Sample A structure: A thin layer of $CH_3NH_3PbI_3$ (500 nm) is deposited by spin coating on a Si/SiO_2 substrate, a previous buffer of TiO_2 was deposited on SiO_2 to enhance the HPVK adherence. (b) Sample B structure: similar to sample A, but adding a PMMA cladding layer (2.5 µm) on top of the HPVK. (c) and (d) PL spectra for different pump powers in sample A and B, respectively.

5 Electrical Injection of QD-based devices

To make integrated QD-based light sources viable on-chip light sources, electrically driven QD light emitting devices are needed and integration on chip must be demonstrated. Electrically driven light emission by colloidal quantum dots requires the formation of electron-hole pairs in the quantum dots, for example by direct injection of electrons and holes, that subsequently emits light by radiative recombination. Although this is possible utilizing seperate electron and hole contacts, a relatively straightforward approach that is readily amenable to down-scaling and photonics integration is based on sandwiching three or more quantum dot layers in between two insulators to form a quantum dot capacitor. When driving this capacitor using a sufficiently high, alternating voltage, electron injection from the valence band to the conduction band between quantum dots in successive layers occurs and the resulting electron-hole pairs in the central quantum dot layers emit light (as shown in Figure 19).

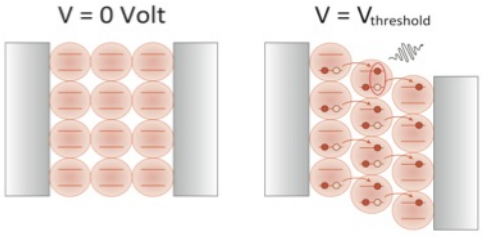

Figure 19: Operation principle of AC driven QD-capacitor

Figure 20: EL from the AC driven sandwich structure: ITO-SiN-QDs-SiN-MC

The sandwich-structure used to demonstrate electroluminescence consist of: a glass substrate with an ITO layer, a SiN layer is deposited on top, followed by a spin-cast CdSe/CdS core-shell QDs layer and another SiN layer, and finally metal contacts. Using metal probe needles an AC voltage can be applied over the QDs (see Figure 20). EL intensity as a function of Vpp over the stack, and frequency is shown in Figure 21 and Figure 22 respectively. By using a broad range of driving voltage and analysing the time-dependent displacement current and light emission we will try to understand the details of the operation mechanism of this light emitting quantum-dot capacitor.

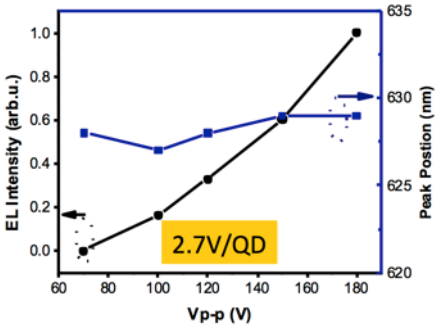

Figure 21: EL intensity vs. Vpp.

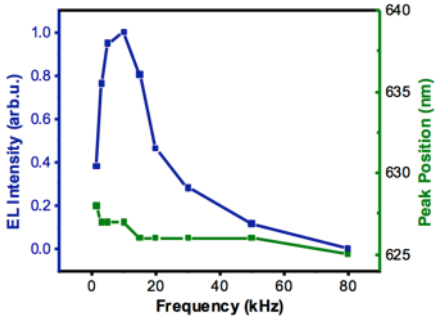

Figure 22: EL intensity vs. modulation frequency AC voltage

6 Conclusion

The objective of this subtask within NAVOLCHI, WP4 was to develop an integrated waveguide amplifier using colloidal quantum dots (CQD) as the active material. This required development of new types of CQDs exhibiting gain in the telecom wavelength range, new waveguide platforms allowing to couple light emitted by the CQDs efficiently to an optical cavity or amplifier and an electrically injection scheme. All of these subtasks were completed succesfully:

- Using a novel material, HgTe, we demonstrated for the first time CQDs exhibiting long-lived gain with ultralow threshold fluence in the wavelength range 1100nm-1600nm. A gain of 100cm-1 is extracted from the measurements (for a close-packed film)
- We developed new platforms, SiN and PMMA based, which allow efficient coupling of CQD-emission to integrated waveguides. We demonstrated gain and lasing in amplifiers and disk resonators fabricated in these systems.
- We demonstrated light extraction from electrically injected stacks of SiN with embedded CQDs

Unfortunately, we did not yet manage to combine all these results in a single device thus far. However, we strongly believe the results achieved in NAVOLCHI form the basis for achieving this in the near future and research towards achieving this continues.

7 References

[1] Q. Li *et al.*, Opt. Express **21**, 18236 (2013).
[2] D. J. Moss *et al.*, Nat. Photonics **7**, 597 (2013).
[3] X. G. Tu *et al.*, Opt. Express **20**, 2640 (2012).
[4] B. De Geyter *et al.*, Appl. Phys. Lett. **101** (2012).
[5] S. Gupta, and E. Waks, Opt. Express 21, 29612 (2013).
[6] M. Cirillo et al., Chem. Mater. 26, 1154 (2014).
[7] I. Suárez, E. J. Juárez-Pérez, I. Mora-Seró, J. Bisquert and J. P. Martínez-Pastor, Polymer/perovskite amplifying waveguides for active hybrid silicon photonics, Advanced Materials, in press (2015).
[8] Z. Ning et al., Quantum-dot-in-perovskite solids, Nature 523, 324 (2015)

8 Most relevant publications arising from this work

[1] W. Xie, Y. Zhu, Tangi Aubert, S. Verstuyft, Zeger Hens, D. Van Thourhout, Low-Loss Silicon Nitride Waveguide Hybridly Integrated With Colloidal Quantum Dots, Optics Express, 23(9), United States, p.12152-12160 (2015)

[2] A. Omari, W. Xie, P. Geiregat, D. Van Thourhout, Z. Hens, Modeling the optical properties of low-cost colloidal quantum dot functionalized strip SOI waveguides, Journal of Selected Topics in Quantum Electronics, 99, (2013).

[3] P. Geiregat, A.J. Houtepen, F.C. Grozema, D. Van Thourhout, Z. Hens, Picosecond All-Optical Wavelength Conversion using Hot Carrier Intraband Absorption in Colloidal PbS Nanocrystals , submitted for publication in Nanoletters.

[4] Yolanda Justo, P. Geiregat, Karen Van Hoecke, Frank Vanhaecke, Celso de Mello Donga, Zeger Hens, Optical Properties of PbS/CdS Core/Shell Quantum Dots, Journal of Physical Chemistry C, 117(39), p.20171–20177 (2013)

[5] A. Omari, P. Geiregat, D. Van Thourhout, Z. Hens, Light absorption in hybrid silicon-on-insulator/quantum dot waveguides, Optics Express, 21(20), p.23272-23285 (2013)

[6] P. Geiregat, Y. Justo, S. Flamee, S. Abe, Z. Hens, Giant and Broadband Absorption Enhancement in Colloidal Quantum Dot Monolayers through Dipolar Coupling, ACS Nano, 7(2), p.987–993 (2012)

[7] W. Xie, Y. Zhu, Tangi Aubert, Zeger Hens, Edouard Brainis, D. Van Thourhout, On-chip Hybrid Integration of Silicon Nitride Microdisk With Colloidal Quantum Dots, accepted for publication in 12th International Conference on Group IV Photonics

[8] W. Xie, D. Van Thourhout, Fabrication of high-Q silicon nitride microdisk resonator coupled with on-chip waveguide, Proceedings of the 19th Annual Symposium of the IEEE Photonics Society Benelux Chapter, Netherlands, p.145-148 (2014)

[9] W. Xie, D. Van Thourhout, High-Q Free-standing Silicon Nitride Microdisk Vertically Coupled with On-chip Waveguide, CLEO 2014, United States, (2014)

[10] Y. Zhu, W. Xie, S. Verstuyft, Tangi Aubert, Zeger Hens, D. Van Thourhout, Colloidal quantum dot silicon nitride platform, Proceedings of the 2013 Annual Symposium of the IEEE Photonics Society Belenux Chapter, Netherlands, p.175-178 (2013).

[11] P. Geiregat, C. Delerue, Y. Justo, M. Aerts, F. Spoor, D. Van Thourhout, L. D. Siebbeles, G. Allan, A.J. Houtepen, Z. Hens, A Phonon Scattering Bottleneck for Carrier Cooling in Lead-Chalcogenide Nanocrystals, accepted for publication in E-MRS Spring Meeting, France

[12] P. Geiregat, A.J. Houtepen, F. Grozema, D. Van Thourhout, Z. Hens, Picosecond All-Optical Wavelength Conversion using Hot Carrier Intraband Absorption in Colloidal Nanocrystals, accepted for publication in E-MRS Spring Meeting, France

[13] P. Geiregat, A.J. Houtepen, F.C. Grozema, D. Van Thourhout, Z. Hens, Picosecond All-Optical Wavelength Conversion using Hot Carrier Intraband Absorption in Colloidal PbS Nanocrystals , MRS Spring Meeting - WW4.04, United States, (2015)

[14] P. Geiregat, C. Delerue, Y. Justo, M. Aerts, F. Spoor, D. Van Thourhout, L. Siebbeles, G. Allan, A.J. Houtepen, Z. Hens, A Phonon Scattering Bottleneck for Carrier Cooling in Lead-Chalcogenide Nanocrystals, MRS Spring Meeting - U1.08, United States, (2015)

[15] P. Geiregat, A. Houtepen, D. Van Thourhout, Z. Hens, Low Power All---Optical Wavelength Conversion with Terahertz Refresh Rates using Colloidal Nanocrystals, CLEO Europe, Germany, 2015

[16] P. Geiregat, A. Houtepen, L.K. Sagar, C. Delerue, G. Allan, D. Van Thourhout, Z. Hens, Thresholdless Optical Gain using Colloidal HgTe Nanocrystals, CLEO, United States, p.paper FtH4C4 (2014)

[17] P. Geiregat, A. Houtepen, C. Delerue, G. Allan, L.K. Sagar, D. Van Thourhout, Z. Hens, Near-Thresholdless Optical Gain using Colloidal HgTe Nanocrystals, 30 Years of Colloidal Quantum Dots, (2014).

[18] Z. Hens, A. Omari, P. Geiregat, D. Van Thourhout, Optical Properties of SOI Waveguides Functionalized with Close-Packed Quantum Dot Films, 15th International Conference on Transparent Optical Networks (ICTON 2013), Spain, p.paper We.D6.2 (2013)

[19] P. Geiregat, A. Omari, Yolanda Justo, D. Van Thourhout, Zeger Hens, Absorption Enhancement in 2D Nanocrystal Superlattices through Near-Field Dipolar Coupling: A Novel Optical Phenomenon at the Nanoscale, Laser Science to Photonics Applications (CLEO 2013), United States, p.paper QTu1A.7 (2013)

[20] Omari, P. Geiregat, D. Van Thourhout, Z. Hens, Modelling colloidal quantum dots on SOI photonic waveguides, EMRS 2013 Spring & Bilateral, (2013).

[21] Omari, P. Geiregat, D. Van Thourhout, Z. Hens, Probing the optical constants at the nanoscale of colloidal prepared films through optical waveguides., NWO Scientific meeting on Chemistry related to Physics & Material Sciences, Netherlands, (2013).

[22] P. Geiregat, Y. Justo, S. Abe, S. Flamee, Z. Hens, Giant and Broadband Absorption Enhancement in Colloidal Nanocrystal Superlattices through Dipolar Coupling, EMRS Spring Meeting, France, (2013).

[23] H. Gordillo, I. Suárez, R. Abargues, P. Rodríguez-Cantó, S. Albert and J.P. Martínez-Pastor, Polymer/QDs nanocomposites for wave-guiding applications, Journal of Nanomaterials, **Vol. 2012**, Article ID 960201 (doi:10.1155/2012/960201), 1-9 (2012).

[24] H. Gordillo, I. Suárez, R. Abargues, P. Rodríguez-Cantó and J.P. Martínez-Pastor, Color tuning and white light by dispersing CdSe, CdTe and CdS in PMMA nanocomposite waveguides, IEEE Photon. J. **5**, 2201412 (12 pgs) (2013).

[25] H. Gordillo, I. Suárez, R. Abargues, P. Rodríguez-Cantó, G. Almuneau and J. P. Martínez-Pastor, Quantum-dot double layer polymer waveguides by evanescent light coupling, IEEE/OSA J. of Lightwave Technol. **31**, 2515-2525 (2013).

[26] I. Suárez, H. Gordillo, R. Abargues, P. Rodríguez-Cantó, S. Albert and J.P. Martínez-Pastor, Dielectric and plasmonic waveguides based on quantum dots embedded in polymers, Opt. Pura Apl. 46, 303-308 (2013).

[27] I. Suárez, A. Larrue, P.J. Rodríguez-Cantó, G. Almuneau, R. Abargues, V. S. Chirvony and J.P. Martínez-Pastor, Efficient excitation of photoluminescence in a two-dimensional waveguide consisting of a QD-polymer heterostructure, Optics Letters **39**, 4692-4695 (2014).

[28] I. Suárez, E. J. Juárez-Pérez, I. Mora-Seró, J. Bisquert and J. P. Martínez-Pastor, Polymer/perovskite amplifying waveguides for active hybrid silicon photonics, Advanced Materials, in press (2015).